Effects of Wavelength Change
in Holographic Reconstructions

R. W. Menzel
ARO, Inc.

August 1981

Final Report for Period October 1978 — September 1979

**ARNOLD ENGINEERING DEVELOPMENT CENTER
ARNOLD AIR FORCE STATION, TENNESSEE
AIR FORCE SYSTEMS COMMAND
UNITED STATES AIR FORCE**

This report has been reviewed by the Office of Public Affairs (PA) and is releasable to the National Technical Information Service (NTIS). At NTIS, it will be available to the general public, including foreign nations.
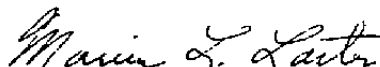
APPROVAL STATEMENT

This report has been reviewed and approved.

MARSHALL K. KINGERY
Directorate of Technology
Deputy for Operations

Approved for publication:

FOR THE COMMANDER

MARION L. LASTER
Director of Technology
Deputy for Operations

REPORT DOCUMENTATION PAGE		READ INSTRUCTIONS BEFORE COMPLETING FORM
1 REPORT NUMBER AEDC-TR-79-84	2 GOVT ACCESSION NO.	3 RECIPIENT'S CATALOG NUMBER
4 TITLE (and Subtitle) EFFECTS OF WAVELENGTH CHANGE IN HOLOGRAPHIC RECONSTRUCTIONS		5 TYPE OF REPORT & PERIOD COVERED Final Report - October 1978 - September 1979
		6 PERFORMING ORG REPORT NUMBER
7 AUTHOR(s) R. W. Menzel, ARO, Inc., a Sverdrup Corporation Company		8 CONTRACT OR GRANT NUMBER(s)
9 PERFORMING ORGANIZATION NAME AND ADDRESS Arnold Engineering Development Center/DOT Air Force Systems Command Arnold Air Force Station, Tennessee 37389		10 PROGRAM ELEMENT, PROJECT, TASK AREA & WORK UNIT NUMBERS Program Element 65807F
11 CONTROLLING OFFICE NAME AND ADDRESS Arnold Engineering Development Center/DOS Air Force Systems Command Arnold Air Force Station, Tennessee 37389		12 REPORT DATE August 1981
		13 NUMBER OF PAGES 30
14 MONITORING AGENCY NAME & ADDRESS(if different from Controlling Office)		15 SECURITY CLASS (of this report) UNCLASSIFIED
		15a DECLASSIFICATION DOWNGRADING SCHEDULE N/A

16 DISTRIBUTION STATEMENT (of this Report)

Approved for public release; distribution unlimited.

17 DISTRIBUTION STATEMENT (of the abstract entered in Block 20, if different from Report)

18 SUPPLEMENTARY NOTES

Available in Defense Technical Information Center (DTIC).

19 KEY WORDS (Continue on reverse side if necessary and identify by block number)

holography	numerical analysis
wavelength change	infrared equipment
resolution	lasers
reconstruction	

20 ABSTRACT (Continue on reverse side if necessary and identify by block number)

    Holographic imaging is necessary in some particulate measurements in test facilities at AEDC. Additionally, projection of holographic images of infrared (IR) test objects is being considered to enhance the IR sensor test capability at AEDC. Lasers of different wavelengths often are necessary in the recording and reconstruction of the required holograms. As a result, a study of the effects of a wavelength change between the recording and reconstruction illumination on the aberration, resolution, and location of holographically

DD FORM 1473 EDITION OF 1 NOV 65 IS OBSOLETE
1 JAN 73

20. ABSTRACT (Continued)

reconstructed images was experimentally undertaken. Control of aberration and resolution degradation, to the extent possible, is described.

AFSC
Arnold AFS Tenn

PREFACE

The work reported herein was conducted by the Arnold Engineering Development Center (AEDC), Air Force Systems Command (AFSC). The results of the research were obtained by ARO, Inc., AEDC Division (a Sverdrup Corporation Company), operating contractor for the AEDC, AFSC, Arnold Air Force Station, Tennessee, under ARO Project Number P32L-02. The Air Force project manager was M. K. Kingery, Directorate of Technology. The manuscript was submitted for publication on September 28, 1979.

Dr. R. W. Menzel is currently employed by Calspan Field Services, Inc., AEDC Division.

CONTENTS

ILLUSTRATIONS

TABLES

1.0 INTRODUCTION

## 1.1 IMPETUS FOR THE WORK EFFORT

A wavelength change between the recording and reconstruction illumination of a hologram causes degrading changes in the information content of the reconstructed images. There are two problem areas for the study of wavelength change influences in holography — resolution in particle-field holography and reconstruction of holographic images with infrared (IR) illumination. The problem addressed in this report is to characterize these changes and to specify their alleviation when possible.

The wind tunnels and engine test cells at the Arnold Engineering Development Center (AEDC) routinely operate with solid-particle and liquid-droplet fields in order to simulate desired atmospheric conditions for testing operational characteristics and material reliability of aerodynamic systems. Holography has proved to be a viable technique for calibrating and analyzing the particle and droplet fields (Ref. 1). The principal advantages of applying holography for particle-field analysis are twofold. First, a three-dimensional instantaneous recording of the particle field is obtained without disturbing the field. Second, an after-the-fact study of the field characteristics, such as size and spatial distribution, shape factors, number density, and velocity, can be made.

Particle-field holocameras use a pulsed ruby laser (wavelength 694.3 nm). The pulse duration is typically 10 to 20 nsec, which allows "stop action" recording of particles that may have very high velocities. The reconstructed images are formed using a continuous-wave laser, typically the helium-neon (He-Ne) laser (wavelength 632.8 nm). The wavelength change causes the reconstructed images to undergo a magnification change, a shift in their physical location, and aberration degradation that reduces the resolution with which the particles may be recognized.

Figure 1 illustrates the resolution problem. Both holograms were recorded with the same holocamera but with different recording wavelengths (λ_r). The object field is an Ealing dot and line comparison reticle. The reconstruction wavelength (λ_c) of both images is the same but resulted in a wavelength change of 61.5 μm for the image in Fig. 1a and no wavelength change for the image in Fig. 1b. In addition to the apparently decreased quality of Fig. 1a, microscopic examination shows that Fig. 1b allows resolution of a 10-μm-diam particle but the resolution in Fig. 1a is no better than 15 μm. This degrading difference is attributed to the wavelength change in the holographic reconstruction and possibly to multimoding in the ruby laser line structure.
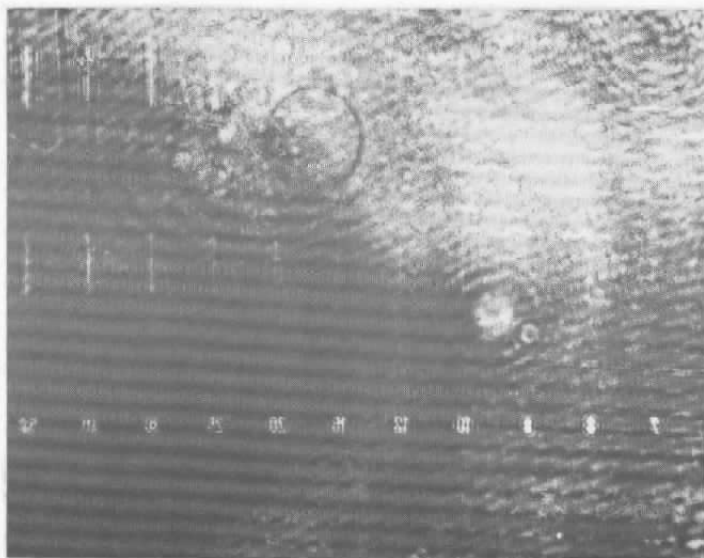
a. λ_r = 694.3 nm
λ_c = 632.8 nm
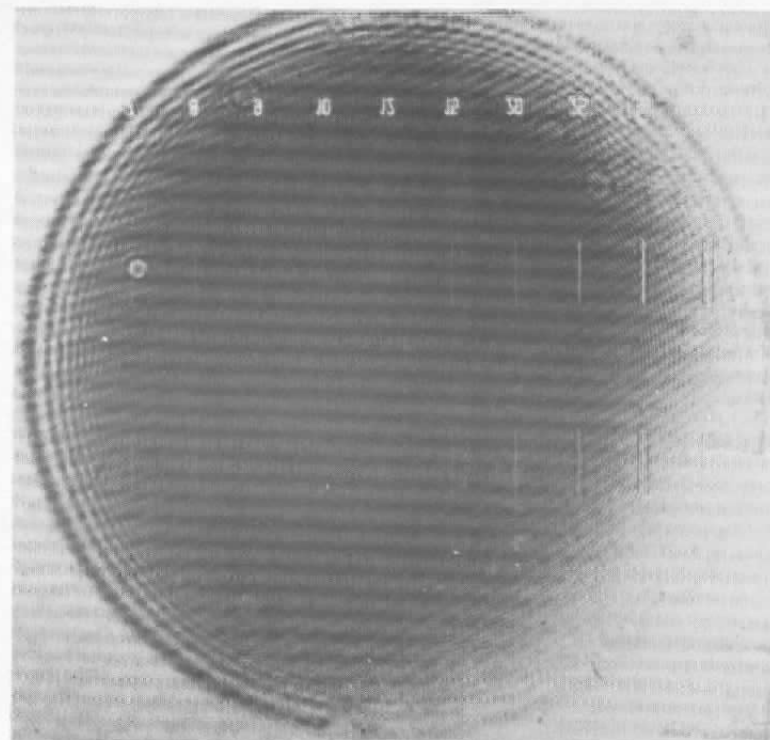
b. λ_r = 632.8 nm
λ_c = 632.8 nm

Figure 1. Reconstructed image degradation as encountered in a particle field holocamera.

Apart from the particle-field holography are the problems of holographic construction of IR images. These problems are addressed in response to interest at the AEDC in the use of IR projection techniques for studying state-of-the-art IR sensors in space chambers. Holographic IR imaging is being developed because the techniques provide the potential for recording three-dimensional images and because the images may be projected into the test chamber without the IR noise that accompanies actual IR-emitting objects on support stands. This situation is depicted in Fig. 2. Normally, the IR target simulation equipment consists of a radiation source assembly and a collimating mirror (Ref. 2), as shown in Fig. 2a. Holography allows an image to be projected within the chamber as shown in Fig. 2b. The advantages offered are (a) less IR background noise is generated because the images are free-standing in space, (b) less cryogenic cooling is necessary because the IR sources are outside the chamber, and (c) the image configuration can easily be changed without interrupting the chamber environment.

Most of the problems with IR holography are caused by the lack of suitable recording materials. Although many materials have been used in the infrared (Ref. 3), they either do not provide satisfactory results or are in an early stage of experimental development. A review of photosensitive materials for holographic recording (Ref. 4) indicates that "although special photographic emulsions with spectral sensitivities for the infrared region up to about 1.3 μm are available, their MTF (modulation transfer function) and granularity characteristics make them unsuitable for recording holograms with radiation of 1.06 μm from Nd:YAG lasers." Some holographic emulsions are sensitive to the Herschel reversal effect (Ref. 3); however, the sensitivity to IR radiation was about six orders of magnitude lower than for visible light. Additionally, the MTF of this technique restricts the spatial frequency to less than about 50 lines/mm, which is not adequate for high-resolution holography.

Therefore, IR holography at the AEDC will be pursued as follows. Holograms will be recorded on conventional holographic films in the visible spectrum. Because the film plates are not transparent past about 2 μm, the holograms will be made reflective by vacuum depositing a thin layer of aluminum on the film emulsion. This uses to advantage the developed emulsion shrinkage that geometrically contours the surface to conform with the exposed density levels. The surface is effectively a grating that, by reflection, produces interferometric field constructions to produce an image. The major constraint in this method is that reconstruction wavelengths greater than the grating spacing will not diffract (Ref. 5). For a recording wavelength, λ_r, the grating spacing is given by $\lambda_r/2 \sin(\theta/2)$ where θ is the angle between the object and the reference beams in the recording. If the reconstruction wavelength is λ_c, then for
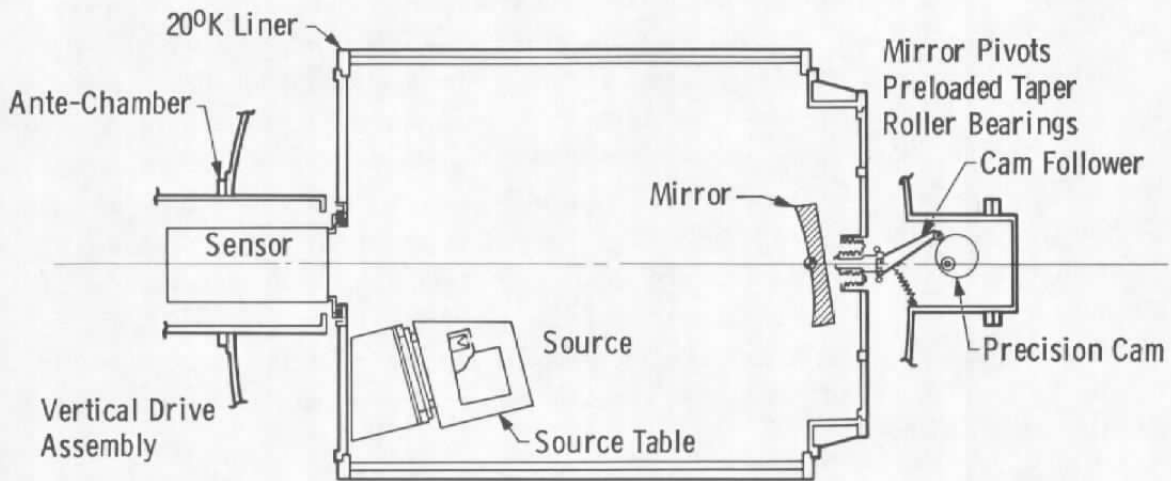
a. Conventional infrared source
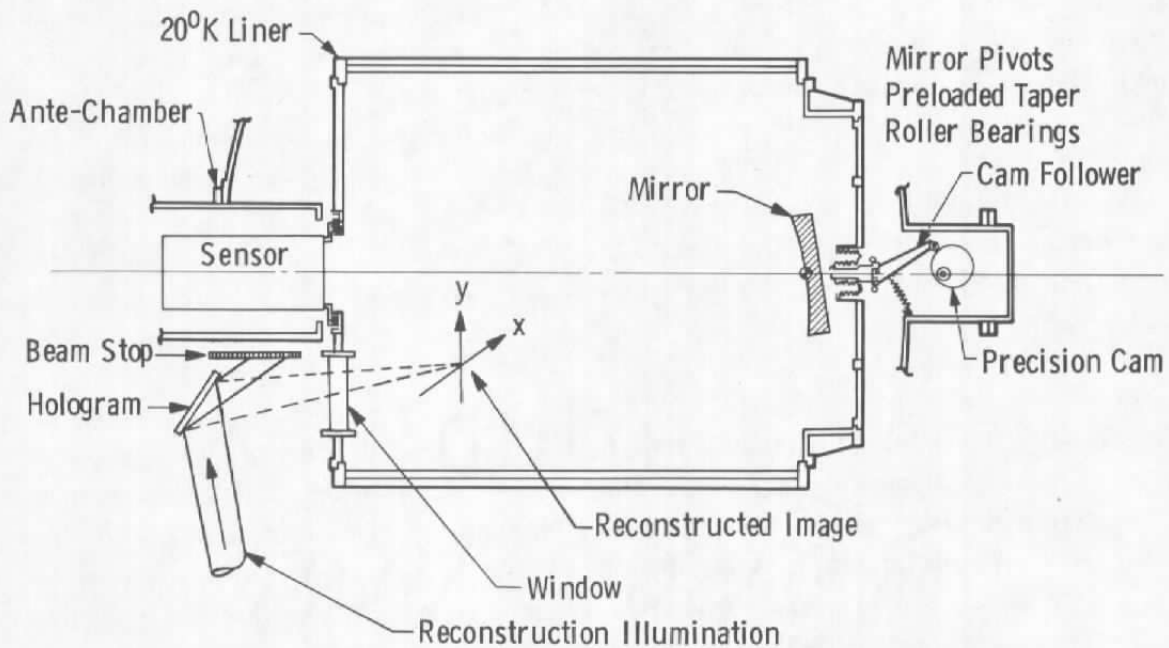
b. Holographic infrared source
Figure 2. Comparison of conventional and holographic sources
for the sensor test chamber.

8

$$\lambda_r / \lambda_c \leq 2 \sin (\theta/2) \tag{1}$$

reconstruction diffraction will occur. Therefore, the desired wavelength ratio sets boundaries on the permissible recording geometry.

Once again, a wavelength change is an essential ingredient of the technique and image degradations result. As a prelude to the study of IR images with all its attendant image conversion difficulties, a study of image changes in the visible region may be used to infer the degrading changes that may be expected in the near-IR region.

1.2 APPROACH TO THE PROBLEM

Reconstructed image information degradations were divided into three categories: image aberrations, overall resolution changes, and geometrical location of the images. These effects were studied by recording holograms at wavelengths of 476.2 (blue), 530.9 (green), 568.2 (yellow), and 647.1 nm (red). The holograms were reconstructed at each of these wavelengths plus two additional laser lines at 482.5 and 520.8 nm.

Aberration-related degradations in point spread functions were experimentally obtained. Sample calculations of aberrations for several holocamera geometries showed their respective advantages and disadvantages.

Resolution as a function of wavelength change for particle images and bar chart images were obtained. Resolution is found to be dependent on the image shape. A qualitative explanation of their differences is given.

Experimental determination of the geometrical location of the wavelength-changed reconstructed images are presented. These are shown to follow theoretical predictions very closely.

2.0 HOLOGRAPHIC ABERRATIONS

2.1 ABERRATIONS IN HOLOGRAPHIC RECONSTRUCTIONS

The imaging, magnification, and aberration properties of holography have been derived for the paraxial case by Meier (Ref. 6) and for the nonparaxial case by Champagne (Ref. 5). Both cases are similar and are derived by assuming point source radiation fields:

$$E_q = (A_q/r_q) \exp\left\{i\ (2\pi/\lambda_q)\ r_q\right\}\tag{2}$$

where the subscript q is a generalization of the specific subscripts o, r, c, and i that, respectively, are the object, reference, reconstruction, and image fields; A_q is an amplitude; r_q is a distance (for example, r_o is the distance between the object point and the holographic film plane); and λ_q represents the wavelength. The imaging and aberration properties are derived from a comparison of the exponential phase term of the reconstructed image field to an idealized point source. The phase terms are expanded in a power series about r_q using the coordinate systems as defined in Fig. 3. It should be noted that the reconstruction plane illumination (x_c, y_c, z_c) is not shown in Fig. 3 because it is very similar to the reference plane illumination (x_r, y_r, z_r).
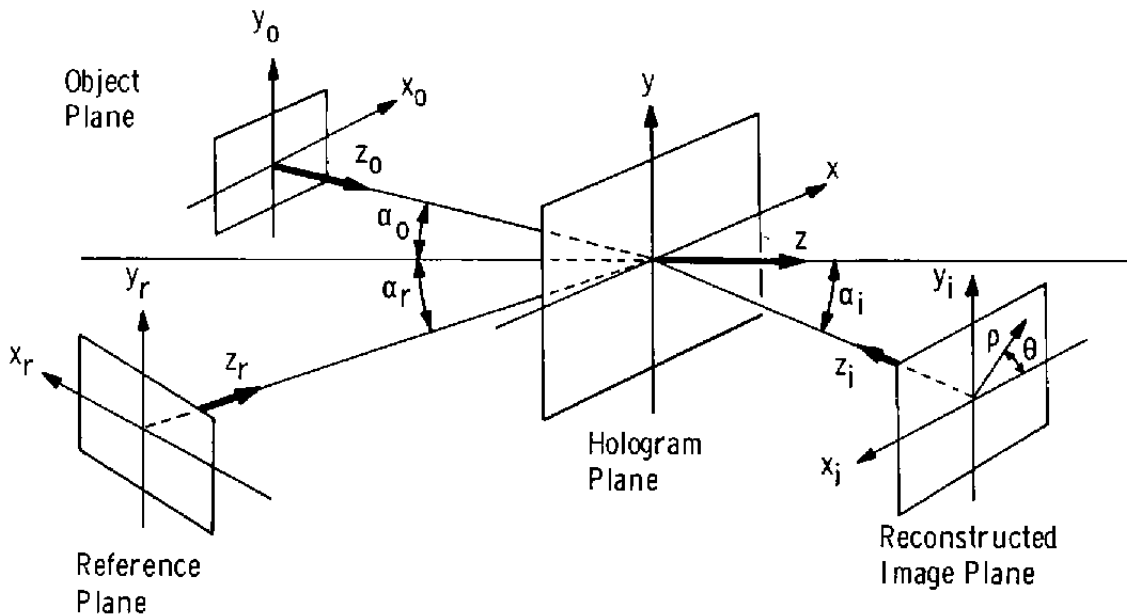
Note: The reconstruction illumination plane (x_c, y_c, z_c) is similar to the reference plane.

Figure 3. Holographic recording and reconstruction geometry.

The resulting image location and magnification are:

Focus Condition:

$$\frac{1}{z_i} = \frac{1}{z_c} \pm \left(\frac{\mu}{m^2}\right)\left(\frac{1}{z_o} - \frac{1}{z_r}\right) \tag{3}$$

Orientation Condition:

$$\sin \alpha_i = \sin \alpha_c \pm \left(\frac{\mu}{m^2}\right)(\sin \alpha_o - \sin \alpha_r) \tag{4}$$

Lateral Magnification:

$$M_{lat} = m \Bigg/ \left[1 \pm \left(\frac{m^2}{\mu}\right)\frac{z_o}{z_c} - \frac{z_o}{z_r}\right]^{-1} \tag{5}$$

Longitudinal Magnification:

$$M_{long.} = \frac{1}{\mu} M_{lat}^2 \tag{6}$$

where $\mu = \lambda_c/\lambda_r$ and m is a scale increase or decrease of the hologram dimensions.

The aberrations of the reconstructed image phase term is

$$\Phi_i = \frac{2\pi}{\lambda_c}\left[-\frac{1}{8}\rho^4 S + \frac{1}{2}\rho^3 C \cos\theta - \frac{1}{2}\rho^2 A \cos^2\theta\right] \tag{7}$$

where S, C, and A are, respectively, the spherical, coma, and astigmatism coefficients given by

$$S = \frac{1}{z_c^3} = \left(\frac{\mu}{m^4}\right)\left(\frac{1}{z_o^3} - \frac{1}{z_r^3}\right) - \frac{1}{z_i^3} \tag{8}$$

11

$$C = \frac{\sin \alpha_c}{z_c^2} \pm \left(\frac{\mu}{m^3}\right) \left(\frac{\sin \alpha_o}{z_o^2} - \frac{\sin \alpha_r}{z_r^2}\right) - \frac{\sin \alpha_i}{z_i^2} \tag{9}$$

$$A = \frac{\sin^2 \alpha_c}{z_c} \pm \left(\frac{\mu}{m^2}\right) \left(\frac{\sin^2 \alpha_o}{z_o} - \frac{\sin^2 \alpha_r}{z_r}\right) - \frac{\sin^2 \alpha_i}{z_i} \tag{10}$$

For simplicity (without interfering in the general case) it has been assumed that y_o, y_r, y_c, and y_i are approximately zero. The ($\pm$) notations in the above equations refer to the real image (-) and the virtual image (+).

Two other forms of aberration — distortion and field curvature — are not included in this description "...because these aberrations do not degrade the sharpness of an image, but only influence its location... In this formulation, the object and images were considered to be point sources, so that relative position has no meaning... (Ref. 5).

Considerable simplification (both mathematical and experimental) results if plane collimated waves are used for the reference and the reconstruction illuminations. Then $z_r = z_c = \infty$. Together with the experimental condition of considering only the real image, there results:

Focus Condition:

$$\frac{1}{z_i} = - \left(\frac{\mu}{m^2}\right) \frac{1}{z_o} \tag{11}$$

Orientation Condition:

$$\sin \alpha_i = \sin \alpha_c - \left(\frac{\mu}{m}\right) (\sin \alpha_o - \sin \alpha_r) \tag{12}$$

Lateral Magnification:

$$M_{lat} = m \tag{13}$$

Longitudinal Magnification:

$$M_{long.} = \frac{m^2}{\mu} \tag{14}$$

Spherical Aberration:

$$S = -\frac{\mu}{m^4} \frac{1}{z_o^3} \left[1 - \left(\frac{\mu}{m}\right)^2 \right] \tag{15}$$

Coma:

$$C = -\frac{\mu}{m^3} \frac{1}{z_o^2} \left[\sin \alpha_o + \left(\frac{\mu}{m}\right) \sin \alpha_i \right] \tag{16}$$

Astigmatism:

$$A = -\frac{\mu}{m^2} \frac{1}{z_o} \left[\sin^2 \alpha_o - \sin^2 \alpha_i \right] \tag{17}$$

2.2 MINIMIZING ABERRATIONS

The holocamera geometries that have different degrees of aberration are presented. First, consider the case where the reference beam and the reconstruction beam are both perpendicular to the hologram plane (i.e., $\alpha_r = \alpha_c = 0$). Using the focus and orientation conditions, the aberrations become

$$S = -\frac{\mu}{m^4} \frac{1}{z_o^3} \left[1 - \left(\frac{\mu}{m}\right)^2 \right] \tag{18}$$

$$C = -\frac{\mu}{m^3} \frac{1}{z_o^2} \sin \alpha_o \left[1 - \left(\frac{\mu}{m}\right)^2 \right] \tag{19}$$

$$A = -\frac{\mu}{m^2} \frac{1}{z_o} \sin^2 \alpha_o \left[1 - \left(\frac{\mu}{m}\right)^2 \right] \tag{20}$$

13

This case has the advantage of eliminating all of the aberrations simultaneously, but only when the hologram size is scaled by the ratio of the reconstruction and recording wavelengths, μ. Since hologram scaling requires additional processing steps that introduce noise, scaling is not particularly desirable. The noise effects of scaling are offset, however, because the easily obtained, accurate alignment of the perpendicular reconstruction beam minimizes searching for the best reconstruction alignment. The importance of accurate reconstruction alignment cannot be overstated. Champagne (Ref. 7) found tolerences of less than ± 15 sec of arc necessary for optimizing the resolution.

For the second case, let the object beam be perpendicular to the film plane. Then $\alpha_o = 0$ and

$$S = -\frac{\mu}{m^4} \frac{1}{z_o^3} \left[1 - \left(\frac{\mu}{m}\right)^2 \right] \tag{21}$$

$$C = -\frac{\mu}{m^4} \frac{1}{z_o^2} \left[\sin \alpha_c + \left(\frac{\mu}{m}\right) \sin \alpha_r \right] \tag{22}$$

$$A = -\frac{\mu}{m^3} \frac{1}{z_o} \left[\sin \alpha_c + \left(\frac{\mu}{m}\right) \sin \alpha_r \right]^2 \tag{23}$$

Although the three aberrations cannot be simultaneously eliminated, coma and astigmatism vanish by aligning the reconstruction beam such that the bracketed term reduces to zero. This requires a conjugate beam (i.e., $\alpha_c \approx -\alpha_r$) and an angular displacement from the recording geometry determined by (μ/m).

The hologram is actually a three-dimensional recording within the emulsion thickness of the interferometric field (Ref. 8). Diffraction planes are formed within the emulsion depth, and generally these planes are physically shifted by film shrinkage during the development process. If, however, the hologram plane normal bisects the angle between the object and the reference beam, the resulting fringes are nearly perpendicular within the emulsion and film shrinkage effects are minimized. For this case let $\alpha_o = -\alpha_r = \alpha$ so that

$$S = -\frac{\mu}{m^4} \frac{1}{z_o^3} \left[1 - \left(\frac{\mu}{m}\right)^2 \right] \tag{24}$$

$$C = -\frac{\mu}{m^3}\frac{1}{z_o^2}\left\{\left[1 - 2\left(\frac{\mu}{m}\right)^2\right]\sin\alpha + \left(\frac{\mu}{m}\right)\sin\alpha_c\right\}. \tag{25}$$

$$A = -\frac{\mu}{m^2}\frac{1}{z_o}\left\{\sin^2\alpha - \left[\sin\alpha_c - 2\left(\frac{\mu}{m}\right)\sin\alpha\right]^2\right\} \tag{26}$$

Now aberrations cannot be reduced unless $(\mu/m) = 1$ and $\alpha_c = \alpha$ simultaneously. Film scaling is again necessary; without it, aberration-free images are attainable only if there is no wavelength change.

For convenience, the conditions under which aberrations are minimized are synoptically presented in Table 1.

2.3 SAMPLE ESTIMATIONS OF RECONSTRUCTION ABERRATIONS

In anticipation of experimental results, some sample calculations of the aberration magnitudes were made for the three cases described above. These are tabulated in Table 2. For these calculations, the angle between object and reference beams was chosen to be 10 deg, the reconstruction angle was equal to the reference angle, and the image dimension was approximated to be 1 cm at a recording distance of 30 cm. It should be noted that although the recording geometry changes only by the angle with which the film plane intersects the object and reference beams, the resulting aberrations are considerably different. For the $\alpha_r = \alpha_c = 0$ case the aberrations are the least even though they cannot be eliminated without film scaling. For the $\alpha_o = 0$ case, the aberrations are the largest and would render this hologram the most susceptible to image degradation through misalignment of the reconstructing beam. Finally, in all cases spherical aberration contributes the least significant portion of the total aberration and astigmatism the greatest.

2.4 EXPERIMENTAL RESULTS

All of the experimental data in this report result from very similar holocamera geometries. Thus, the reference and reconstruction beams were plane collimated waves ($z_r = z_c = \infty$), the object distance z_o was typically 30 to 35 cm, the angle between object and reference beams was 10 deg, and generally the object beam was perpendicular to the film plane. The film used was Agfa Gavaert 8E75.

15

Table 1. Requirements for Eliminating Aberrations.

Aberration	Reference Beam Perpendicular to Film Plane	Object Beam Perpendicular to Film Plane	Film Plane Normal Bisects Angle Between Object and Reference Beams
Spherical	$\mu/m = 1$	$\mu/m = 1$	$\mu/m = 1$
Coma	$\mu/m = 1$	$\sin \alpha_c = -\mu/m \sin \alpha_r$	$\mu/m = 1$ and $\alpha_c = \alpha_o$
Astigmatism	$\mu/m = 1$	$\sin \alpha_c = -\mu/m \sin \alpha_r$	$\mu/m = 1$ and $\alpha_c = \alpha_o$

Conditions: $z_r = z_c = \infty$

Table 2. Estimation of Reconstruction Aberrations.

Aberration	Referance Beam Perpendicular to Film Plane $\alpha_o = 10$ deg	Object Beam Perpendicular to Film Plane $\alpha_c = \alpha_r = 10$ deg	Film Plane Normal Bisects Angle Between Object and Reference Beams $-\alpha_o = \alpha_r = \alpha_c = 5$ deg
Spherical $\quad \rho^4 \, S/8\lambda$	0.112 Wavelengths	0.112 Wavelengths	0.112 Wavelengths
Coma $\quad \rho^3 \cos\theta \; C/2\lambda$	2.34 Wavelengths	8.84 Wavelengths	1.85 Wavelengths
Astigmatism $\quad \rho^2 \cos^2\theta \; A/2\lambda$	12.2 Wavelengths	79.9 Wavelengths	30.8 Wavelengths

Estimation Conditions:

$\rho = 1$ cm
$\cos\theta = 1$
$m = 1$
$z_o = 30$ cm

$z_r = z_c = \infty$
$\lambda_c = 476.2$ nm
$\lambda_r = 647.1$ nm

To test for the influence of curvature of field distortion the following experiment was made. Holograms were recorded of a set of pinholes arranged in a plane in the shape of a cross. In the reconstructed image the focal position of each pinhole was measured as precisely as the reconstructed focal depth of field would allow. The intention of this exercise was to map out the curvature of the surface on which the reconstructed images lie. The effort was not successful. Repeated measurements yielded random results. The consequent interpretation is that the focal depth of field masks whatever curvature of field may have been present.

Aberrations resulting from a wavelength difference between λ_c and λ_r in the reconstructed image of a 10-μm-diam pinhole are shown in Fig. 4. The size of the pinhole is sufficiently small that the images may be considered to represent the point spread function of the holocamera system. The reconstruction beam angle, α_c, was held constant as λ_c was changed, i.e., there was no effort to correct for the aberrations. Microscopic examination of the images showed recognizable coma and astigmatism.

When α_c was adjusted to satisfy

$$\sin \alpha_c = -\frac{\mu}{m} \sin \alpha_r \qquad (27)$$

the aberration was greatly reduced, as shown in Fig. 5. Some coma is still present, possibly because of film shrinkage effects. The aberration reduction shown in Fig. 5 can also be easily obtained by visually monitoring the image while performing the realignment. As a consequence, it is recommended that holographic recordings include, whenever possible, a recognizable object source. A pinhole is highly suitable as even small changes in the alignment cause substantial visual changes in the reconstructed image.

Equation (27) is compared with experimentally determined angle orientation differences, $\Delta\alpha_c$, which result in best images versus the wavelength change $\Delta\lambda = |\lambda_c - \lambda_r|$ in Fig. 6. The somewhat high readings for the $\lambda_r = 476.2$ nm hologram were probably caused by systematic errors. The figure shows that aberration correction for an arbitrary wavelength change can be obtained by reconstruction realignment with the appropriate $\Delta\alpha_c$. The realignment prediction is important for IR reconstruction where direct visualization may not be available.

18
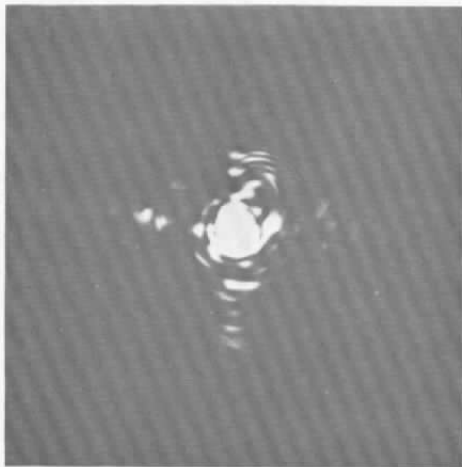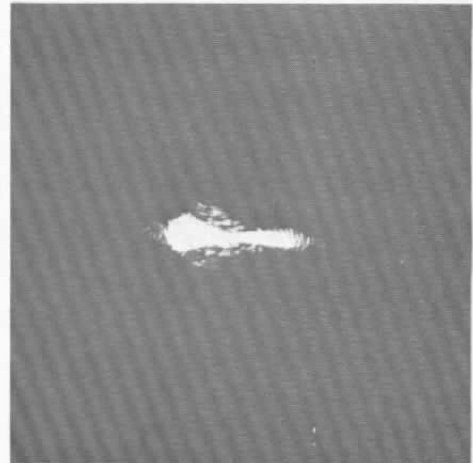
a. $\lambda_c = 647.1$ nm

b. $\lambda_c = 568.2$ nm
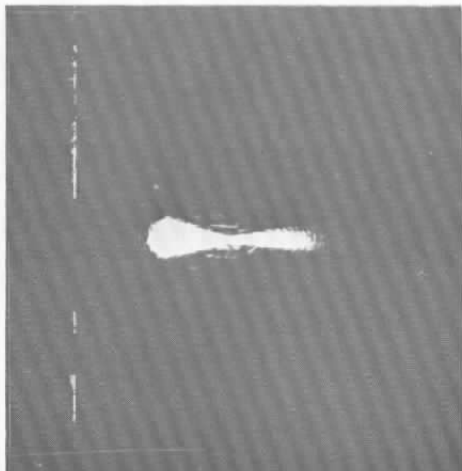
c. $\lambda_c = 530.9$ nm
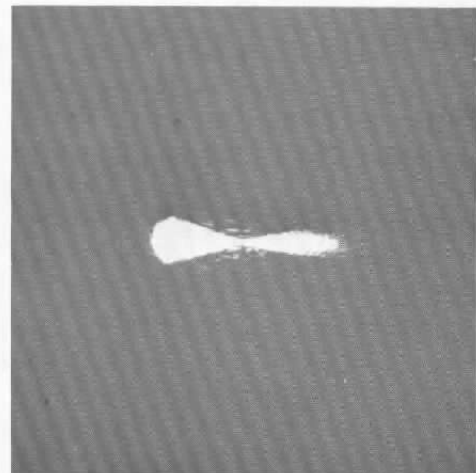
d. $\lambda_c = 476.2$ nm

Notes: Recording wavelength $\lambda_r = 647.1$ nm for all images.
The (a) image is magnified 4x larger than the other images.

Figure 4. Point spread function degradation in holographic reconstructions.

λ_c = 647.1 µm
λ_r = 647.1 µm
α_c = 10.0 deg
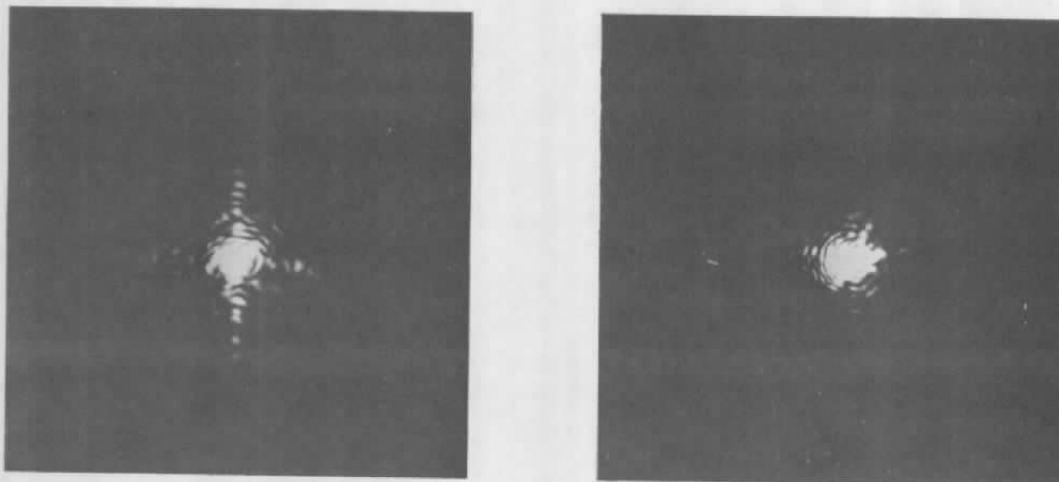
λ_c = 476.2 µm
λ_r = 647.1 µm
α_c = 7.34 deg
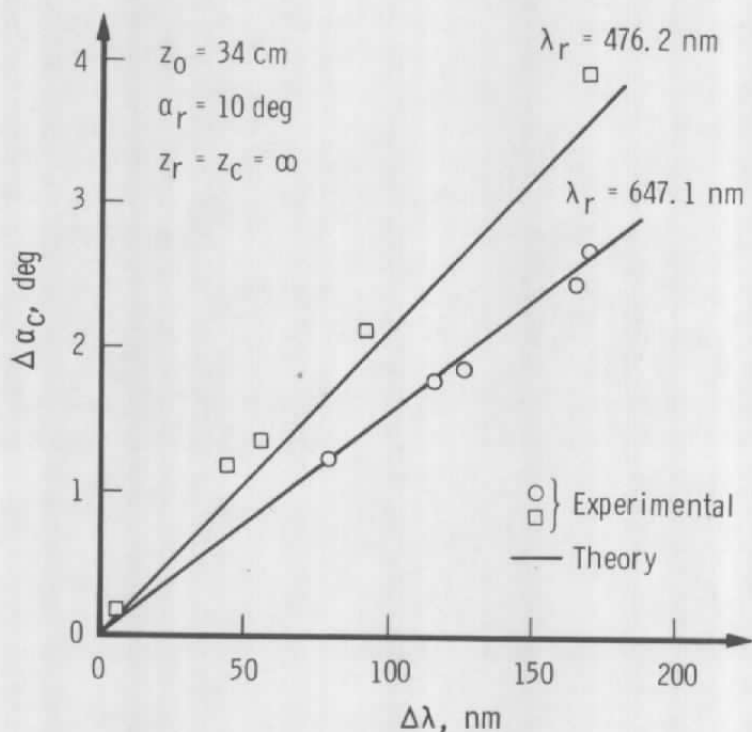
Figure 5. Alignment correction of aberrations.

Figure 6. Angle change between recording and reconstruction versus wavelength change needed to obtain the best images.

3.0 HOLOGRAPHIC RESOLUTION

3.1 WAVELENGTH-CHANGE-DEPENDENT RESOLUTION

Resolution degradation resulting from wavelength changes are qualitatively shown in Fig. 7. The object was a precision resolution target (USAF-1951 MIL. STD. 150-A; 5.1.1.7). The magnification of these reconstructed images is indicated by the square between the numbers 4 and 5, which on the resolution target is 140 μm long on each side. The resolution of 5- to 10-μm line widths within the line groups were observed.

Resolution, despite the ubiquitous use of the Rayleigh criterion, lacks a universally applicable definition. This is demonstrably so because resolution judgment is dependent on the observers' foreknowledge of the image to be recognized and on the shape of the object. To demonstrate this latter point, resolution observations of reconstructed images of the Ealing dot and line comparison reticle were made. The holocamera parameters were the same as described above. The results are incorporated in Fig. 8 and can be summarized as follows:

1. Reconstruction of the narrowest line available (3-μm width, 2-mm length) were recognizable in all the reconstructions independently of the wavelength change. Aberrations were present, but recognition was not in doubt.

2. Dot images of 12-μm diameter were visible for $\Delta\lambda = 0$ and increased to 25- to 30-μm diameter for $\Delta\lambda = 171$ nm. For smaller dot sizes than the 12-μm diameter, the holocamera was "blind", i.e., no suggestion of an image could be recognized. This must be contrasted with:

3. Bar chart images (the USAF-1951 resolution target) were resolvable for widths at 5 μm for $\Delta\lambda = 0$, which increased to about 9 μm for $\Delta\lambda = 171$ nm.

Thus, for bar charts with their rectangular object shapes, smaller line widths are recognizable than for dot (i.e., particle) images. Furthermore, with increasing $\Delta\lambda$, resolution degrades more rapidly for circular, symmetrical objects than for linearly symmetrical objects.

Some explanation for these phenomena are in the diffraction and recording physics (Ref. 9) and can be outlined as follows:

1. The diffracted energy varies as the square of the object's geometrical cross section. Because of their length, resolution limited linear objects often have
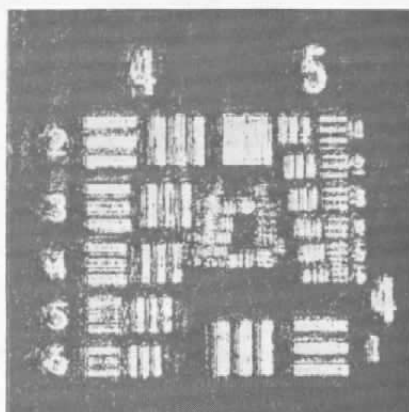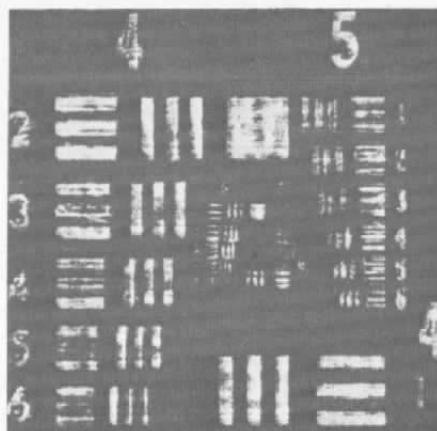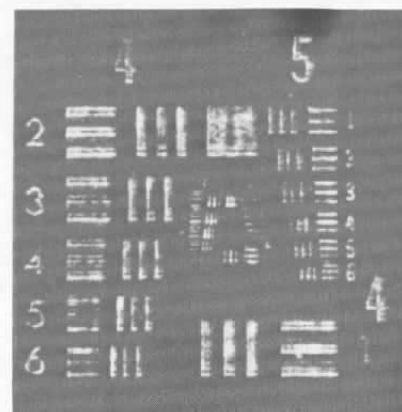
a. $\lambda_c = 647.1$ nm   b. $\lambda_c = 530.9$ nm   c. $\lambda_c = 476.2$ nm
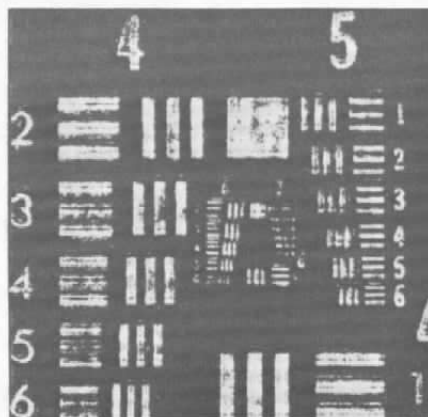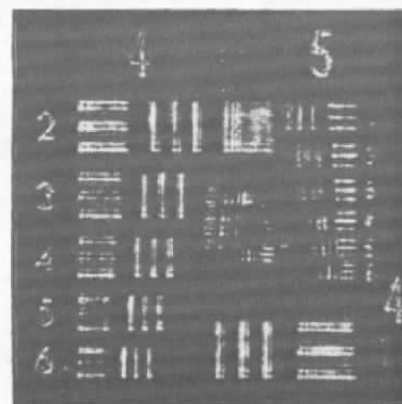
d. $\lambda_c = 568.2$ nm   e. $\lambda_c = 476.2$ nm
a_c adjusted for best image

Notes: Recording wavelength $\lambda_r = 568.2$ nm for all images.

Figure 7. Resolution losses in a bar chart image reconstruction.
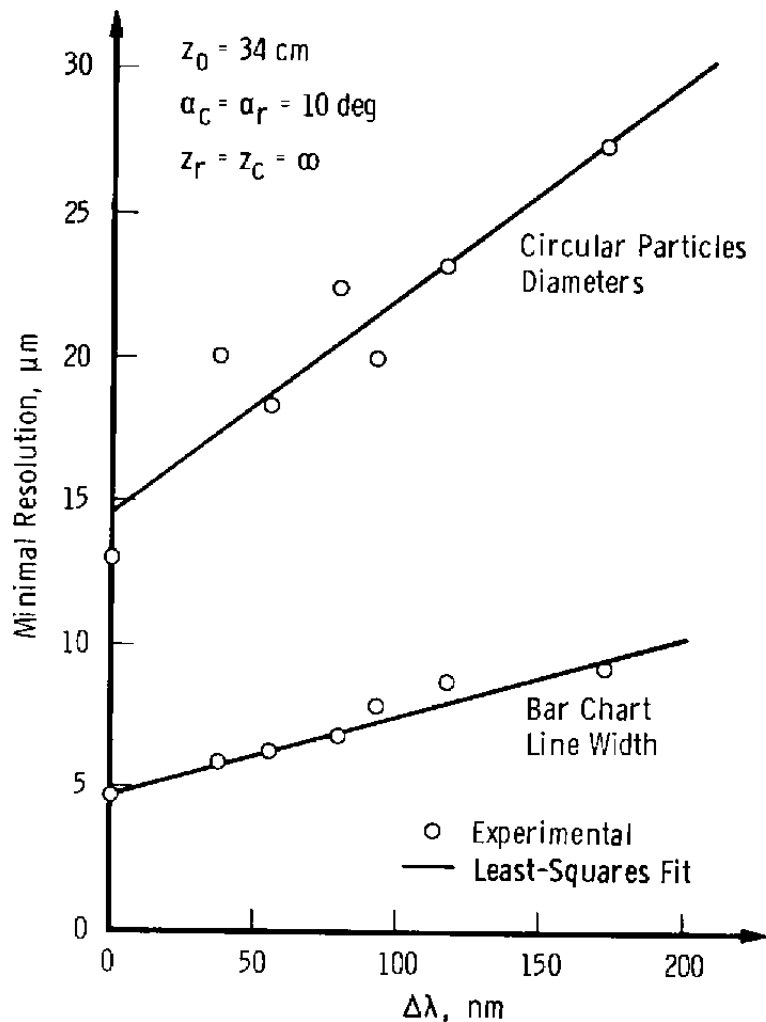
Figure 8. Resolution losses versus reconstruction wavelength change.

larger cross sections than circular objects. This is exemplified by the Ealing target lines.

2. The diffraction intensity varies for circular objects as the first-order Bessel function divided by its argument [$J_1(x)/x$], whereas for linear objects intensity varies as the $\sin(x)/x$ function. Because $J_1(x)$ decreases in amplitude with increasing x, $J_1(x)/x$ will decay more quickly than $\sin(x)/x$. Consequently, the ratio of diffracted energy to the reference beam energy decreases more rapidly for circular objects than for linear objects. The limitations imposed by the film's amplitude response signal-to-noise ratio will cause less diffracted information from the circular object to be recorded than from a comparably dimensioned

linear object. Therefore, the effective size of the hologram of a circular object will be less than for a comparable linear object. This becomes the limiting aperture on the reconstruction resolution.

3. Good visual definition of edge detail in the reconstructed image requires the recording of higher order diffraction fringes. This also explains the improved resolution of larger objects. As the object dimensions increase the diffractive fringe distribution becomes more compact and the amplitude response increases to improve the signal-to-noise ratio. A limit in the sharpness of the edge detail is encountered when the diffraction fringes have a higher spatial frequency than is capable by the film response.

4. For a given hologram size, the energy in the reconstructed image is greater for the linear object than for the circular object. Furthermore, the spread function for objects with circular symmetry is about 18 percent "broader" than for objects with linear symmetry, i.e., the energy density is less.
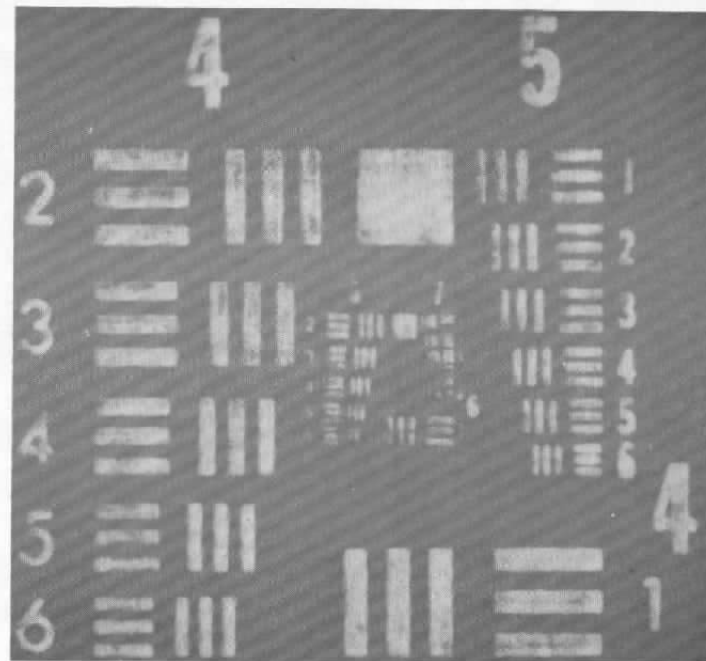
3.2 HOLOGRAPHIC IMAGING CAPABILITIES

From the foregoing discussion, it may seem that the diffraction and film properties set unique limitations on holographic imaging. Such is not the case. A generalized derivation of the mathematical properties of the holographic reconstruction (Ref. 9) shows that governing equations are identical in form with the mathematics describing a lens. In other words, the intensity field in the focused region of the reconstructed image of a point source is identical in form to the intensity field near the focal volume of a diffraction-limited lens. This result is quite important since it places holographic imaging as an equal member in the larger class of optical imaging systems.

Figure 9 shows the similarity of the optical quality of lens and holographic imaging. The object distance z_0 was 11.4 cm, the angles α_0, α_r, and α_c were each 15 deg, and λ_r and λ_c were 632.8 nm. Figure 9 reinforces the contention that holography may be considered as a comparable imaging system rather than unique unto itself, and that the mechanisms of wave-front shaping—reflective, refractive, or defractive—are in themselves not uniquely deciding factors of image quality.

In the same manner, holography is not capable of better resolution than a lens system, nor can resolution past a certain value be recovered in the reconstruction by attention to geometry, wavelength, or optical filtering. It is generally simpler to design a holocamera system with resolution better than required for some application than to recover the theoretical resolution of any particular system.
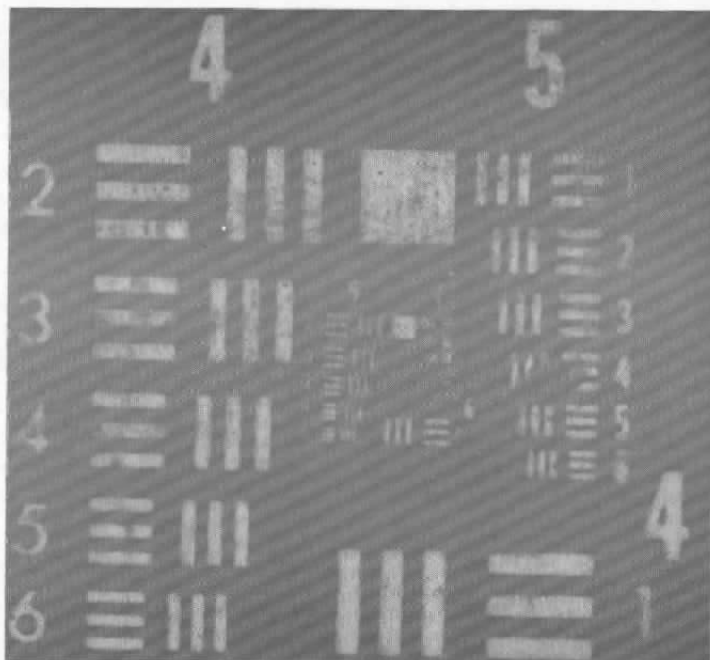
Photographic Image   Off-Axis Reconstructed Image

Figure 9. Comparison of optical and holographic imaging.

4.0 RECONSTRUCTED IMAGE LOCATION

A priori knowledge of the image location when reconstructing in the infrared is important as it may be necessary to accurately position the infrared sensing element. The image locations are described by Eqs. (11) and (12). From Eq. (11) there results

$$
dz_i = \frac{m^2}{\mu^2} \frac{d\lambda}{\lambda_r} z_o \tag{28}
$$

which is the change in focal location caused by a change in the reconstructing wavelength. This effect is certainly not negligible as can best be shown by an example (which was also observed experimentally). For an object distance of $z_o = 35$ cm, scale factor $m = 1$, $\lambda_r = 530.9$ nm, and $\lambda_c = 520.8$ nm ($\Delta\lambda$ is only 101 Å), one obtains $dz_i = 6.92$ mm.

Equation (12) in differential form,

$$
d\left(\sin \alpha_i - \sin \alpha_c\right) = \frac{1}{m} \frac{d\lambda}{\lambda_r} \left(\sin \alpha_r - \sin \alpha_o\right) \tag{29}
$$

emphasizes that a change in image location caused by the wavelength change $d\lambda$ is also dependent on the reconstruction angle and its change. If α_c is held constant and if $d\alpha_i$ is approximated by $\Delta x_i/z_i$ then

$$
\frac{\Delta x_i}{z_i} = \frac{\sin \alpha_c}{\sin \alpha_i} + \frac{1}{m} \frac{1}{\cos \alpha_i} \frac{\Delta\lambda}{\lambda_r} \left(\sin \alpha_r - \sin \alpha_o\right) \tag{30}
$$

The $\Delta\lambda$ term has little effect for relatively small α_i, α_r, α_c, and α_o. This is shown in Fig. 10. The reconstructed image positions from four holograms, each reconstructed at six wavelengths, are plotted. The straight-line fit to the data points shows that the $\Delta\lambda$ term was negligible. Conversely, using the slope of the line and the approximation $\alpha_i = 10$ deg, then

$$
\sin \alpha_c = \left(\frac{\Delta x_i}{z_i}\right) \cos \alpha_i \tag{31}
$$

gives $\alpha_c = 10.08$ deg. This compares favorably with the actual value of $\alpha_c = 10.0$ deg.
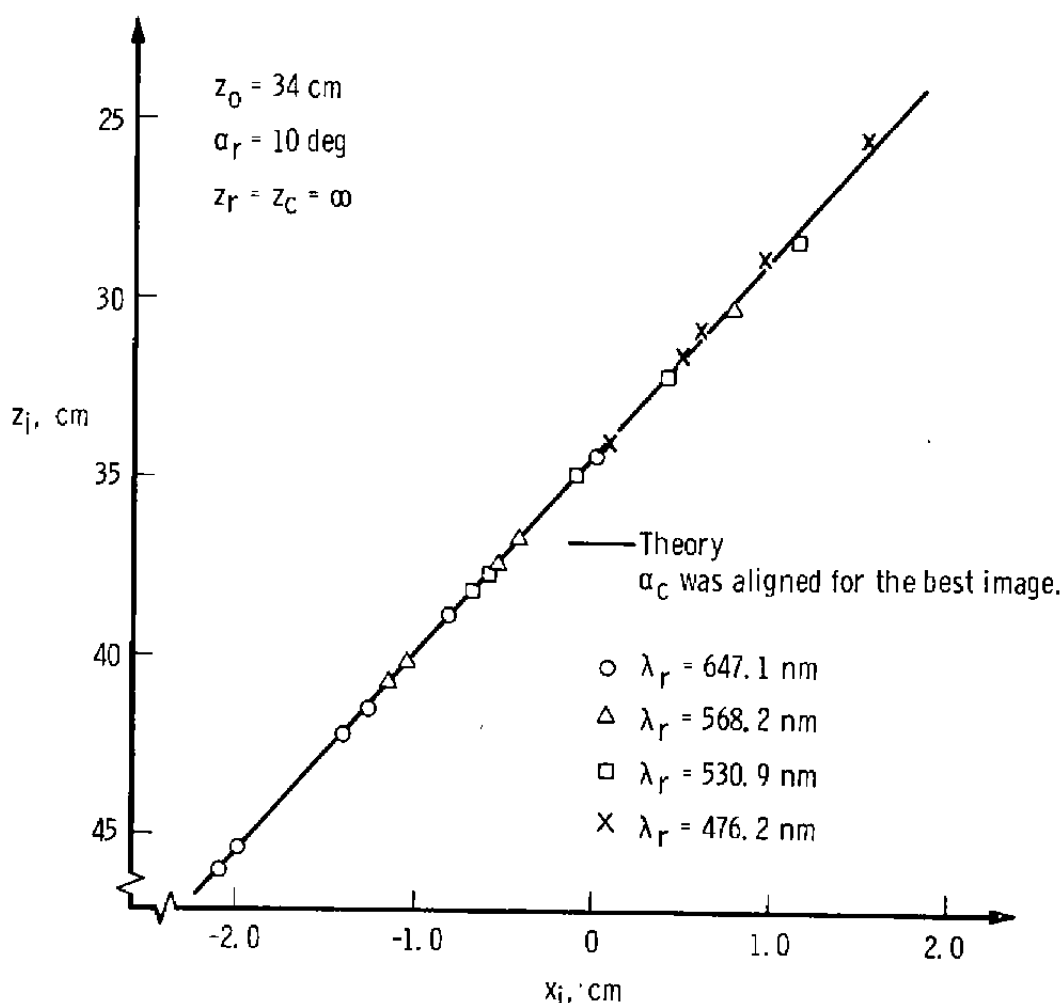
Figure 10. Reconstructed image location.

These examples and Fig. 10 show that although a wavelength change in the reconstruction can cause a considerable change in image position, the position's coordinates can be readily calculated.

5.0 SUMMARY

The degree of aberration in the reconstructed image can be controlled to some extent by the recording geometry. Of the geometries considered, the lowest amount of aberration results when the reference beam is perpendicular to the film plane. Full correction for this case can only be accomplished by scaling the hologram size by the wavelength ratio. On the other hand, full correction for coma and astigmatism is available through reconstruction alignment when the object beam is perpendicular to the film plane. If correct alignment is

not realizable, however, this case produces the worst aberrations. Either way, full aberation correction is generally not available because of emulsion shrinkage during the development process. The residual aberration observed was mainly astigmatism.

Resolution as a function of wavelength change was observed to be different for particle images and bar chart images. Whereas bars with widths as small as 5 μm were observed, the same holocamera became "blind" to particles smaller than about 15 μm. This is largely due to the energies in the respective diffraction patterns that result in the holographic recording. The arcane nature of resolution is further demonstrated in that the rate of resolution loss with wavelength change is different for the two types of images, with particle images suffering greater information loss than the bar images. Resolution degradations in the holographic process are not easily controlled. Rather, it is to greater advantage to strive to obtain a system resolution that is more than required than to recover resolution losses caused by wavelength change.

The geometrical location of the reconstructed image is readily predicted and found if the parameters of the recording geometry are well controlled. Compared with aberration and resolution, the geometrical location is the easiest to predict when projecting a wavelength change into the IR region.

Further work on aberration and resolution control suggested by this study is to obtain experimentally wavelength-ratio-scaled holograms and study their reconstructed images, and to construct a better theoretical model for the resolution losses, especially of particle images. An approach to the latter problem is to solve mathematically the reconstruction diffraction equations and to observe the influence of parametric changes.

REFERENCES

1. Belz, R. A. and Menzel, R. W. "Particle Field Holography at Arnold Engineering Development Center." *Optical Engineering*, Vol. 18, May-June 1979, pp. 256-265.

2. Arnold, F. and Nelms, F. W. "AEDC Long Wavelength Infrared Test Facilities." *Optical Engineering*, Vol. 15, November-December 1976, pp. 549-553.

3. Graube, A. "Infrared Holograms Recorded in High-Resolution Photographic Plates with the Herschel Reversal." *Applied Physics Letters*, Vol. 27, No. 3, August 1975, pp. 136-137.

4. Gladden, J. W. "Review of Photosensitive Materials for Holographic Recordings." Report Number ETL-0128 (AD-A055013), U. S. Army Engineer Topographic Laboratories, Fort Belvoir, Virginia, April 1978.

5. Champagne, E. B. "Nonparaxial Imaging, Magnification, and Aberration Properties in Holography." *Journal of the Optical Society of America*, Vol. 57, No. 1, January 1967, pp. 51-55.

6. Meier, R. W. "Magnification and Third-Order Aberration in Holography." *Journal of the Optical Society of America*, Vol. 55, No. 8, August 1965, pp. 987-992.

7. Champagne, E. B. and Massey, N. G. "Resolution in Holography." *Applied Optics*, Vol. 8, No. 9, September 1969, pp. 1879-1885.

8. Smith, H. M. *Principles of Holography*. John Wiley and Sons, New York, 1975.

9. Menzel, R. W. "Fundamental Properties of Holographically Reconstructed Images." Ph.D. Dissertation in Physics, University of Tennessee, December 1975.

NOMENCLATURE

A   Amplitude, astigmatism coefficient

C   Coma coefficient

M   Magnification

m   Scale increase or decrease of the hologram dimensions

r   Distance

S   Spherical coefficient

x,y,z Plane illuminations

α Beam angle

θ Angle between the object being recorded and the reference beam in the recording

λ Wavelength

μ Ratio of the reconstruction and recording wavelengths, λ_c/λ_r

Φ Reconstructed phase term

SUBSCRIPTS

c   Reconstruction

i   Image

lat   Lateral

long.   Longitudinal

o   Object

q   Generalization of subscripts o,r,c, and i

r   Reference